

INFRARED STUDY OF RECLUSE SPIDER SILK

Patrick McArdle¹, Q.Wang², S.Wang¹, Z.Xing¹, R.Wilmington¹, H.C.Schniepp²,
M.M.Qazilbash¹

¹Department of Physics, The College of William and Mary

²Department of Applied Science, The College of William and Mary

I am reporting the study of single strands of Recluse spider silk with an Infrared Microscope. Silk is relevant for study due to its potential for high impact applications, arising from exceptional mechanical properties. Silks are semi-crystalline biopolymers, which consist of folded proteins that exist in amorphous or crystalline domains. These secondary structures relate to the observed macroscopic mechanical properties. Recluse silk is unique, due to a rectangular cross section not present in any other observed silks. The simplified structure of the Recluse silk has led to the hypothesis of it being an ideal model amongst silks. Infrared transmission was performed on single strands of this silk to study the composition and orientation of the crystalline and amorphous domains present. These details could provide optimized parameters for the production of high strength silks.

INTRODUCTION

Materials research on novel space age materials is paramount for advancements in aeronautics and space exploration. Of these novel materials, spider silk has numerous high impact technological implications including ultra-strong light weight fabrics, biomedical technologies such as biosensors, and optical applications¹. Artificial silks could decrease payload for space bound NASA missions as well as provide an increase in strength and extensibility over existing materials. Silk's durability and relative invariance to temperatures would allow for use in extreme environments where space bound missions occur². These technologies all align with NASA's research in aeronautics and space technology.

As a recipient of the VSGC graduate fellowship last year, I sought to examine the

protein secondary structure present in recluse spider silk. Establishing the connection between secondary structure content/formation and their influence on macroscopic mechanical properties will assist in artificial production of strong extensible silks. Recluse spider silk is special because of its rectangular cross section not present in any other identified silks. Due to this fiber morphology, the fibers are also much thinner, with overall thickness of about ~55nm and width ~10µm as compared to radii of ~1µm for other studied silks with circular cross-section. Since the morphology of the recluse spider silk is simpler, it is hypothesized that this could be a fundamental silk³. If fully understood, this silk could pave the understanding of all other more complicated biopolymers. In the following sections I will present the work that been completed, and how I propose to extend the research for next year.

Formatted: Indent: First line: 0.5", Line spacing: single

Formatted: Indent: First line: 0", Line spacing: single

EXPERIMENT

Infrared polarized FTIR transmission measurements of multiple and single strand recluse spider have been taken. The multiple strand polarized FTIR infrared transmission data was taken previously by S.Wang and Z.Xing. These multiple strand data sets only provide a qualitative measure of secondary structures present. This is due in part to the difficulty of defining the strand geometry relative to the incident beam in the multiple turn system. For this reason the multiple turn data is not discussed in the main text. Single strand microscopic studies in the infrared provide local quantitative secondary structural information by eliminating this geometrical uncertainty. Local structural information is highly relevant in determining the interplay between the protein secondary structure present and silk's unique macroscopic mechanical properties. Issues arise in obtaining quality microscopic data though, due to the difficulty of attaining high signal to noise for microscope spot sizes in the mid-infrared. This is due to the low throughput of readily available mid-infrared light sources. To circumvent this issue, optimization of the beam path optical alignment, proper choice of limiting aperture size and lengthening acquisition times were necessary to obtain sufficient signal.

We coupled our Bruker 80v FTIR Infrared spectrometer to a Spectratech optical microscope with confocal Schwarzschild objectives of numerical aperture 0.58. We designed and implemented moveable sample and detector stages for optimized precision transmission and reflectance measurements. The whole microscope is encased in a chamber which was filled with ~10 psi of compressed air. This compressed air had been scrubbed of CO₂ and H₂O by our Parker Balston gas

purge. Both CO₂ and H₂O have large absorption lines in the mid-infrared so they must be removed to obtain reliable results free of artificial absorption lines. Our infrared light source is a water cooled globar, and we used a KBr beamsplitter. We polarized our input beam parallel and perpendicular to the long axis of the silk strands with a wire grid KRS-5 polarizer. Each measurement, involved taking data for both polarization states. Data was taken between 1000 cm⁻¹ – 4000 cm⁻¹ with 4 cm⁻¹ spectral resolution using a liquid nitrogen cooled MCT photoconductor. This spectral range captures the Amide I,II, and III regions of interest. The dimensions for a single strand of our silk is ~55 nm thick, and ~ 10 μm wide. The dimensions of these strands was previously measured using AFM topography scans³.

In order to get absolute transmission values, the spot size at the focus of the object needed to be determined. Data was taken with confocal rectangular 0.25 mm x 3 mm apertures, which with 15 times magnification equates to a ~ 16 μm x 200 μm spot at the focus of the object. This aperture size was chosen to maximize the amount single strand in the field of view. It was natural to elongate the apertures along the length of the strand while reducing the width. This allowed us to get sufficient signal-to-noise while maintaining single strand precision. To corroborate the predicted spot size values we measured the beam size along both axes with the knife edge method. This involved scanning a sharp edged knife perpendicular to the optical axis at the focus and measuring the integrated intensity. The results were fit to the following formula⁴

$$P(x) = \frac{A}{2} \left[1 + \operatorname{erf} \left(\frac{\sqrt{2}(x-x_0)}{w} \right) \right] + C \quad (1)$$

where A, C and w in equation 1 are fitting parameters. The spot size is then determined from the fitting parameter w which is the beam waist of the Gaussian beam. The measured spot size is ~2 times larger than the theoretical prediction based on the

A frequency dependent background exists in the transmission spectrum. This background likely occurs as a result of frequency dependent diffraction, reflectance and scattering due to the geometry of the spider silk fiber used for transmission

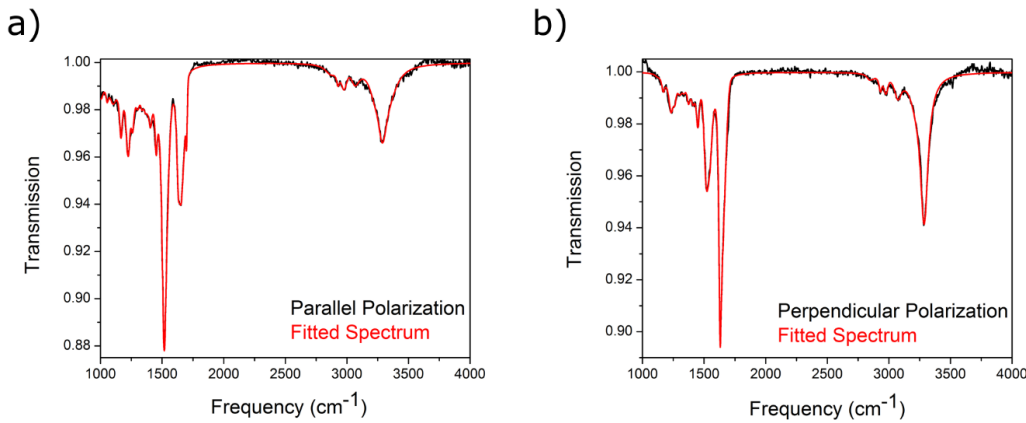


Figure 1: Experimental and oscillator fitted transmission spectra for both polarization states. a) Polarization parallel to the fiber long axis. b) Polarization perpendicular to the fiber long axis.

magnification of our lens, across our spectral range of interest.

Another detail required for absolute data fitting is the incident beam angle. We chose to average the beam angle between our primary aperture axes to simplify the analysis. The angle along the 3 mm axis was determined by measuring the spot size at different stage heights. The half angle for the 3 mm axis was determined to be ~ 20°. The beam angle along the 0.25 mm axis could not be measured directly since the change in spot size at different heights was indiscernible. Instead a calculation was performed to estimate the beam angle. Using étendue conservation and the spot sizes measured with the knife edge method, the approximate half angle was calculated to be ~6.7°. Averaging the results, the beam angle used in data fitting was ~13°.

measurements. We are able to remove this background using the following procedure. We initially exclude the spectral range of infrared vibrational modes, and use a polynomial to fit the remaining featureless spectrum which is mainly attributed to transmission background. We then subtract this polynomial fit from the raw transmission data to obtain a background-free transmission spectrum.

Since our confocal apertures were larger than the fiber being sampled, part of the beam did not pass through the sample. This geometrical mismatch was corrected by weighting the experimental spectrum by a ratio of incident beam powers. The incident beam powers are the power transmitted through the fiber and the total power through the aperture. The powers were calculated by assuming a Gaussian

distributed intensity as was done with knife edge measurements. The integrated power over the aperture was done using the previously measured spot size data.

DATA ANALYSIS

After accounting for the fact that only a fraction of the total power is incident on the silk strand, the spectra for each of the two polarization states were fit individually. We used a combination of Lorentz and Lorentz-Gauss oscillators to fit the frequency dependent complex dielectric function $\epsilon(\nu)$. This fitted function is used to simulate a transmission spectra given in figure 1, for a given thickness and beam angle, which is then compared to the experimental transmission spectra. The oscillator fit parameters are characteristic of the particular type of proteins present, as well as their orientation. The Lorentz model assumes that molecular bonds respond to electrical fields as a driving force on a damped harmonic oscillator^{5,6}, with the equation of motion

$$M \left(\frac{d^2 \bar{u}}{dt^2} \right) - M \gamma \left(\frac{d \bar{u}}{dt} \right) = - M \omega_T^2 \bar{u} + Q E_0 e^{i \omega t} \hat{e} \quad (2)$$

where M is the reduced mass, \bar{u} is the displacement from the equilibrium position, γ is the damping factor, ω_T is the natural frequency of the oscillators, ω is the (angular) frequency of electric field, Q is the charge of the oscillators, E_0 is the amplitude of the electric field, and \hat{e} is the polarization of the incident electric field. The polarization field responds linearly to the displacement, which results in a frequency dependent dispersion relation to govern the propagation of electric fields through the medium. In Tables 1-2 we have referenced our fitted oscillators for both polarization states with

published works, Tables 1-2 are provided at the end.

In

Table 1 and Table 2, we can see that the most prominent molecular assignments of the vibrational modes include beta sheet with polyaniline domains and amides. Beta sheets are one of the main structures we see in the silk. They are the crystalline regions of the silk and are often poly-Ala structures with alanine residues⁷. Beta sheets are very distinct and contain a hydrogen face as well as a methyl and methanolic group comprising another face⁸. They exist on the order of a few nanometers, and consist of a dense network of hydrogen bonds⁹⁻¹¹. A study conducted using electron diffraction on spider dragline silk found the space group of beta sheets to be P2₁¹².

An amide is an organic compound with a general structure that include an O=C—N group. They are amongst the characteristic bands that are regularly found in the infrared spectra of proteins and polypeptides, as they link amino acids. Amide I absorption is associated with

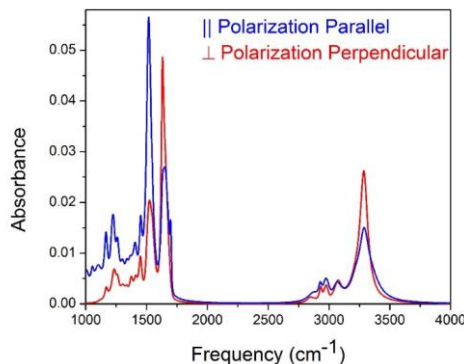


Figure 2: Fitted infrared absorbance spectra for both polarization states. The absorbance was obtained by $A = -\log(T_r)$ where T_r is the fitted transmission spectrum.

stretching vibrations of C=O bonds, while Amide II absorption is associated with bending vibrations of the N—H bond¹³. Amide III is a broad band that is comprised of C—C stretching, C=O stretching, C—N stretching, and N—H bending¹⁴. All of these bonds are important in the hydrogen bonding of the secondary structure of protein. It is important to note that the Amide I band is difficult to resolve because the amplitude is small compared to the intrinsic width of the band—one broad peak is observed instead of many well resolved peaks¹³. We note that another prominent amide, Amide A, occurs between 3270 and 3310 cm⁻¹, depending on the strength of the hydrogen bond¹⁵. Amide A comes from the NH stretching vibration, and is localized on the NH group¹⁵. It occurs as part of the Fermi resonance doublet¹⁵. The second component, amide B, is weaker and occurs between 3030 and 3100 cm⁻¹¹⁵.

Note that we also converted the transmission spectrum to an absorbance spectrum by using the formula $A = -\log\left(\frac{I}{I_0}\right)$, where I_0 is the intensity of the beam transmitted through the reference aperture, and I is the intensity of the beam transmitted through the silk specimen. This formula stems from the Beer-Lambert Law. The absorption spectra are shown in Figure 2. Absorbance allows quantitative characterization of the different chemical quantities in our silk, since it is the absorbance and not the transmission which is proportional to individual concentrations in a sample¹⁶.

In both polarizations, the vibrational modes occur in two distinct groups, one from ~700 to 1700 cm⁻¹, and one from ~2800 to 3300 cm⁻¹. This stems from the $\omega_T^2 = k/M$ relationship, where k is an effective spring constant that signifies the bond strength. The modes at higher frequencies arise from vibrations of lighter

elements, such as hydrogen. Moreover, they originate from stronger chemical bonds with higher effective spring constants and tend to be stretching modes¹⁷. Conversely, modes at lower frequencies arise from heavier elements, such as carbon, nitrogen, and oxygen, and are more likely to be bending modes with lower effective spring constants¹⁷.

The polarized infrared data shows that the silk of the recluse spider is anisotropic because of differences between the spectra for polarizations parallel and perpendicular to the long axis of the silk. There are fewer vibrational modes apparent in the data obtained with polarization perpendicular to the long axis of the silk. Both polarizations show a large mode at ~1500-1600 cm⁻¹ arising from the Amide II structure. However, it is much stronger in the parallel polarization. The parallel polarization shows an additional large mode at ~1660 cm⁻¹. Also note that the N-H stretching Amide A mode at ~3300 cm⁻¹ appears more strongly in the data obtained with polarization perpendicular to the long axis of the silk.

CONCLUSION

In collaboration with Dr. Schniepp's research group in the applied science department at the College of William and Mary, we are in the process of writing a publication. They have performed polarized single strand Raman spectroscopy which will be compared to our single strand infrared data. Based on the mutual exclusion principle for a crystalline material, Raman and Infrared vibrational modes are at distinct non overlapping frequencies because of crystal symmetries¹⁸. For an amorphous material no translational symmetry exists, so all vibrational modes are allowed and

Raman and Infrared modes will overlap. Therefore by comparison of single strand Raman and infrared spectra, we can infer which features in the spectra are crystalline or amorphous. This allows us to make estimates of the crystalline and amorphous composition in our silk. It is known that crystallinity and strength are correlated quantities¹⁹. As previously stated, the recluse spider's silk is potentially a fundamental member of its material class due to its simplified morphology³. Under this hypothesis, the crystalline content of the recluse silk which has not been previously characterized, could be the optimal quantity for biopolymers in general. Establishing the optimal ratio of crystalline to amorphous composition in biopolymers for a given application, will greatly enhance the ability for the production of artificial silks.

ACKNOWLEDGEMENTS

I would like to thank my advisor M.M.Qazilbash for guidance throughout the project. Thanks to our collaborators Q.Wang, H.C.Schniepp for silk samples and topic related discussion. Acknowledgement to S.Wang and Z.Xing for data acquisition and initial analysis of multi-turn data. I would like to thank R.Wilmington for help with coupling the IR microscope to our spectrometer. Lastly, I would like to thank the VSGC for funding this project.

Center Frequency (cm ⁻¹) of infrared modes of recluse spider silk	Molecular Assignment	Frequency from literature
964.21	β-PAla (CH ₃ rock, N-C _α stretch)	963 ²⁰
1002.2	(AlaGly) _n CH ₃ chain	1000 ²⁰
1054	PPro I (C _α -C _β -C _γ stretch), other amino acids	1049 ²⁰
1102	CH ₃ rock, C _α -C _β str.	1106 ²¹
1166	β -PAla (H _α bend, CH ₃ sym. b., C _α -C _β str.)	1167 ²⁰
1218	Amide III β-Sheet	1224 ²²
1229.9	Amide III Random Coil	1235 ²²
1260.5	Amide III α-helix	1265 ²²
1302.2	β -PAla (CN stretch, H _α bend)	1306 ²³
1336.5	CH ₃ sym. bend, H _α bend, NH ipb	1332 ²⁴
1365	H _α bend, NH ipb, CH ₃ sym. bend	1359 ²⁴
1383	CH ₃ sym. bend	1378-1390 ²¹
1405	Poly L-ala(H _α bend, , CH ₃ sym. b., NC _α str.)	1405 ²⁵
1451.5	β -PAla (CH ₃ asym. Bend)	1454 ²⁰
1515	Amide II	1521 ²⁰

1533	H _α bend, NH ipb, CH ₃ sym. bend	1359 ²⁴
1631	Amide I C=O stretching ²⁶ , Random coil	1648 ²⁶
1654	Amide I C=O stretching ²⁶ , 3 ₁₀ Helix	1663 ²⁶
1680	Amide I C=O stretching ²⁶ , β sheet	1683 ²⁶
1698.7 2869.8	Amide I C=O stretching ²⁶ , β sheet	1697 ²⁰ 2874 ²³
2928	Crystalline Polyglycine I (C ^α H asym str)	2929 ²⁷
2976	β -PAla (CH ₃ asymmetric stretch)	2980 ²³
3066.8	Amide B	3030-3100 ¹⁵
3222		
3288	Amide A NH stretching	3300 ²⁶
3349.7		

Table 1: Infrared vibrational modes in the recluse spider silk data for polarization parallel to the long axis of the silk. Molecular assignments are based on values from the literature for similar organic compounds.

Center Frequency (cm ⁻¹) of infrared modes of recluse spider silk	Molecular Assignment	Frequency from literature
1120	NC str., C _α -C _β str.	1116 ²¹
1168.5	β -PAla (C _α -C _β stretch, H _α bend, CH ₃ symmetric angle bend)	1167 ²³
1232	Amide III Random coil	1235 ²²
1263	Amide III α-helix	1265 ²²
1304	β -PAla (CN stretch, H _α bend)	1306 ²³
1337	CH ₂ wagging mode	1338 ²⁷
1374	β -PAla (CH ₃ symmetric angle bend, H _α bend)	1372 ²³
1410	CH ₂ wagging mode	1409 ²⁸
1449	β -PAla (CH ₃ asymmetrical angle bend)	1444 ²³
1518	Amide II CN stretch, NH bending ²⁶	1520 ²⁸
1549	Amide II CN stretch, NH bending	1542 ²⁰
1629.5	Amide I C=O stretching ²⁶	1620-1640 ²⁶
1644	Amide I, Random Coil	1648 ²⁶
1674	Amide I, β -Turn	1665 ²⁶
2792		

2843	β -PAla (C _α -H _α stretch)	2874 ²³
2932	C ^o H asym str	2929 ²⁷
2976	CH ₃ asym str	2970 ²⁴
3073	Amide B	3030-3100 ¹⁵
3220	Amide A NH stretching	3242 ²³
3286	Amide A NH stretching	3285 ²⁸

Table 2: Infrared vibrational modes in the recluse spider silk data for polarization perpendicular to the long axis of the silk. Molecular assignments are based on values from the literature for similar organic compounds.

References

- (1) Ling, S.; Chen, W.; Fan, Y.; Zheng, K.; Jin, K.; Yu, H.; Buehler, M. J.; Kaplan, D. L. Biopolymer Nanofibrils: Structure, Modeling, Preparation, and Applications. *Prog. Polym. Sci.* **2018**, *85*, 1–56.
- (2) Yang, Y.; Chen, X.; Shao, Z.; Zhou, P.; Porter, D.; Knight, D. P.; Vollrath, F. Toughness of Spider Silk at High and Low Temperatures. *Adv. Mater.* **2005**, *17* (1), 84–88.
- (3) Schniepp, H. C.; Koebley, S. R.; Vollrath, F. Brown Recluse Spider's Nanometer Scale Ribbons of Stiff Extensible Silk. *Adv. Mater.* **2013**, *25* (48), 7028–7032.
- (4) González-cardel, M.; Arguijo, P.; Díaz-uribe, R. Gaussian Beam Radius Measurement with a Knife-Edge : A Polynomial Approximation to the Inverse Error Function. *Appl. Opt.* **2013**, *52* (16), 3849–3855.
- (5) P.Yu; M.Cardona. *Fundamentals of Semiconductors*, 3rd ed.: Springer, 2010.
- (6) M.Dressel; Gruner, G. *Electrodynamics of Solids*, 1st ed.; Cambridge University Press, 2002.
- (7) Kubik, S. High-Performance Fibers from Spider Silk. *Angew. Chemie-International Ed* **2002**, *41* (15), 2721–2723.
- (8) Thiel, B. L.; Guess, K. B.; Viney, C. Non-Periodic Lattice Crystals in the Hierarchical Microstructure of Spider (Major Ampullate) Silk. *Biopolymers* **1996**, *41* (7), 703–719.
- (9) Keten, S.; Buehler, M. J. Nanostructure and Molecular Mechanics of Spider Dragline Silk Protein Assemblies. *J.R.Soc.Interface* **2010**, *7*, 1709–1721.
- (10) Keten, S.; Buehler, M. J. Geometric Confinement Governs the Rupture Strength of H-Bond Assemblies at a Critical Length Scale. *Nano Lett.* **2008**, *8* (2), 743–748.
- (11) Keten, S.; Buehler, M. J. Asymptotic Strength Limit of Hydrogen-Bond Assemblies in Proteins at Vanishing Pulling Rates. *Phys. Rev. Lett.* **2008**, *100*, 1–4.
- (12) Thiel, B. L.; Kunkel, D. D.; Viney, C. Physical and Chemical Microstructure of Spider Dragline: A Study by Analytical Transmission Electron Microscopy. *Biopolymers* **1994**, *34* (8), 1089–1097.
- (13) Gallagher, W. *FTIR Analysis of Protein Structure*; Eau Claire, WI, 1997.
- (14) Timasheff, S. N.; Fasman, G. D. *Structure and Stability of Biological Macromolecules*; Marcel Dekker: New York, 1969.
- (15) Barth, A. Infrared Spectroscopy of Proteins. *Biochim. Biophys. Acta* **2007**, *1767*, 1073–1101.
- (16) Griffiths, P.; de Haseth, J. *Fourier Transform Infrared Spectrometry*, 2nd ed.; John Wiley & Sons, Inc: Hoboken, 2007.
- (17) Timasheff, S. .; Fasman, G. . *Structure and Stability of Biological Macromolecules*; Dekker, M., Ed.; New York, 1969.
- (18) Elliott, S. R. *Physics of Amorphous Materials*, 2nd ed.; John Wiley and Sons Inc: New York, 1990.
- (19) Fink, T. D.; Zha, R. H. Silk and Silk-

- Like Supramolecular Materials. *Macromol. Rapid Commun.* **2018**, *39* (17), 1–17.
- (20) Papadopoulos, P.; Solter, J.; Kremer, F. Structure-Property Relationships in Major Ampullate Spider Silk as Deduced from Polarized FTIR Spectroscopy. *Eur. Phys. J. E* **2007**, *24* (2), 193–199.
- (21) Krimm, S.; Bandekdar, J. Vibrational Analysis of Peptides, Polypeptides and Proteins. *Int. J. Pept. Protein Res.* **1980**, *19*, 1–29.
- (22) Ling, S.; Qi, Z.; Knight, D. P.; Shao, Z.; Chen, X. Synchrotron FTIR Microspectroscopy of Single Natural Silk Fibers. *Biomacromolecules* **2011**, *12* (9), 3344–3349.
- (23) Dwivedi, A. .; Krimm, S. Vibrational Analysis of Peptides, Polypeptides, and Proteins. XI. Beta-Poly(L-Alanine) and Its N-Deuterated Derivative. *Macromolecules* **1982**, *15* (1), 186–193.
- (24) Moore, W. H.; Krimm, S. Vibrational Analysis of Peptides, Polypeptides, and Proteins. II. Beta-Poly(L-Alanine) and Beta-Poly(L-Analyglycine). *Biopolymers* **1976**, *15* (12NA-NA-770103-770104), 2465–2483.
- (25) Moore, W. H.; Krimm, S.; Randall, H. M. Vibrational Analysis of Peptides, Polypeptides, and Alan YlgI Ycine). *Biopolymers* **1976**, *15*, 2465–2483.
- (26) Kong, J.; Yu, S. Fourier Transform Infrared Spectroscopic Analysis of Protein Secondary Structures. *Acta Biochim. Biophys. Sin. (Shanghai)*. **2007**, *39* (8), 549–559.
- (27) Moore, W. H.; Krimm, S. Vibrational Analysis of Peptides, Polypeptides, and Proteins. I. Polyglycine I. *Biopolymers* **1976**, *15* (12), 2439–2464.
- (28) Taga, K.; Sowa, M. G.; Wang, J.; Etori, H.; Yoshida, T.; Okabayashi, H.; Mantsch, H. H. FT-IR Spectra of Glycine Oligomers. *Vib. Spectrosc.* **1997**, *14*, 143–146.